Cell, Vol. 114, 445–456, August 22, 2003, Copyright ©2003 by Cell Press

hippo Encodes a Ste-20 Family Protein Kinase that Restricts Cell Proliferation and Promotes Apoptosis in Conjunction with *salvador* and *warts*

Shian Wu,[1,2] Jianbin Huang,[1,2] Jixin Dong,[1] and Duojia Pan[1,*]
[1]Department of Physiology
University of Texas Southwestern Medical Center at Dallas
5323 Harry Hines Boulevard
Dallas, Texas 75390

Summary

The coordination between cell proliferation and cell death is essential to maintain homeostasis within multicellular organisms. The mechanisms underlying this regulation are yet to be completely understood. Here, we report the identification of *hippo* (*hpo*) as a gene that regulates both cell proliferation and cell death in *Drosophila*. *hpo* encodes a Ste-20 family protein kinase that binds to and phosphorylates the tumor suppressor protein Salvador (Sav), which is known to interact with the Warts (Wts) protein kinase. Loss of *hpo* results in elevated transcription of the cell cycle regulator *cyclin E* and the cell-death inhibitor *diap1*, leading to increased proliferation and reduced apoptosis. Further, we show that *hpo*, *sav*, and *wts* define a pathway that regulates *diap1* at the transcriptional level. A human homolog of *hpo* completely rescues the overgrowth phenotype of *Drosophila hpo* mutants, suggesting that *hpo* might play a conserved role for growth control in mammals.

Introduction

During metazoan development, cell-intrinsic and -extrinsic factors act coordinately to specify the characteristic size and number of diverse cell types (Conlon and Raff, 1999; Stocker and Hafen, 2000). The final number of cells in an organ or organism is determined by the balanced act of cell proliferation and cell death (apoptosis). A challenge is to understand how these processes are coordinated in normal development and how aberrant regulation of this coordination leads to pathological conditions such as cancer.

The relationships between cell proliferation and cell death are complex. It has long been observed that increased proliferation due to activation of oncogenes such as Myc or Ras is often accompanied by increased apoptosis (reviewed in Green and Evan, 2002). This has led to the proposal that apoptosis act as a built-in failsafe to prevent "inappropriate" proliferation of somatic cells (Green and Evan, 2002). Thus, sustained growth of cancer cells not only requires activation of the cell proliferation machinery, but also suppression of the apoptotic failsafe mechanisms. In most cases, this is brought about by coupling oncogene activation with antiapoptotic lesions such as overexpression of Bcl-2 or loss of p53 (Green and Evan, 2002). However, it is also possible that there exist gene networks that couple proliferation to apoptosis in such a manner that loss of a single gene may simultaneously promote proliferation and suppress apoptosis.

The compound eye of *Drosophila* provides an excellent model to decipher the mechanisms that coordinate cell proliferation and apoptosis. This highly organized structure develops from the eye imaginal disc wherein cell proliferation and apoptosis occurs in a stereotyped manner (Wolff and Ready, 1993). Cells divide asynchronously during early larval periods. Starting in the mid-third instar larval stage, a morphogenetic furrow (MF) moves across the eye imaginal disc from posterior to anterior. Cells anterior to the MF are undifferentiated and divide asynchronously, whereas cells in the MF are synchronized in the G1 phase of the cell cycle. Posterior to the MF, cells either exit the cell cycle and differentiate or undergo one round of synchronous division (second mitotic wave, SMW) before differentiation. These cells assemble into approximately 750 ommatidia, leaving behind approximately 2000 superfluous cells that are eliminated by a wave of apoptosis ~36 hr after puparium formation (APF) (Wolff and Ready, 1993). Previous studies have identified cyclin E (CycE) and DIAP1 as key regulators of cell cycle and apoptosis, respectively (Richardson et al., 1995; Hay et al., 1995). Cell cycle exit requires the downregulation of CycE/cdk2 activity, while DIAP1 functions by inhibiting the proapoptotic caspases. That coordinated regulation of cyclin E and DIAP1 might play a critical role organ size control is supported by recent studies of the *Drosophila* tumor suppressor gene *salvador* (*sav*, also called *shrp*), which encodes a protein containing WW and coiled-coil domains (Tapon et al., 2002; Kango-Singh et al., 2002). Loss of *sav* leads to increased cell proliferation and decreased apoptosis associated with elevated levels of CycE and DIAP1 proteins. Interestingly, Sav associates with the Warts (Wts, also called Lats) protein kinase, suggesting that Sav and Wts might function in a common signaling pathway (Tapon et al., 2002). Indeed, loss of *wts* also leads to increased cell proliferation and decreased apoptosis (Tapon et al., 2002). At present, little is known about the molecular architecture of this signaling pathway.

In a genetic screen in *Drosophila* for overgrowth mutants, we have identified *hippo* (*hpo*), a gene that promotes both cell cycle exit and cell death. Here, we show that *hpo* encodes a Ste-20 family protein kinase that together with *sav* and *wts* define a signaling pathway that modulates both cell cycle and apoptosis. We also suggest that this pathway might play a conserved role in growth control in mammals.

Results

Isolation of *hpo* Mutants

We used X-ray mutagenesis and FRT/FLP system to screen the *Drosophila* genome for genes that negatively regulate tissue growth. Three lethal mutations, *42–20*,

*Correspondence: dpan@mednet.swmed.edu
[2]These authors contributed equally to this work.

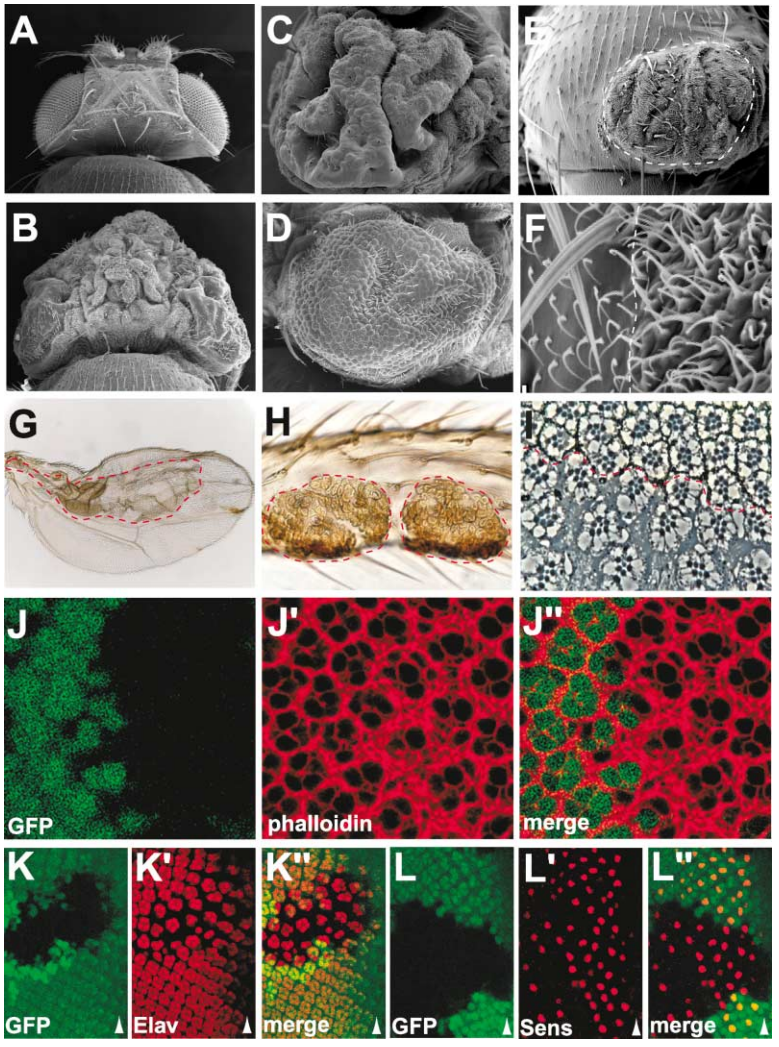

Figure 1. Loss of *hpo* Results in Tissue Overgrowth

(A–B) Scanning electron micrographs (SEM) of a wild-type (A) and a fly head composed predominantly of *hpo* cells (B). The genotypes are (A) *y w ey-flp*; *FRT42D/FRT42D* w^+ *l(2)c1-R11* and (B) *y w ey-flp*; hpo^{42-47} *FRT42D/FRT42D* w^+ *l(2)c1-R11*.

(C) Same as in (B) except that the side view of the compound eye is shown. Note presence of folded eye tissues and a general lack of ommatidia facets.

(D) SEM of a compound eye composed predominantly of hpo^{42-20} mutant cells. The eye is less folded and many ommatidial facets are discernable. The genotype is *y w ey-flp*; hpo^{42-20} *FRT42D/FRT42D* w^+ *l(2)c1-R11*.

(E) SEM of a *Drosophila* notum containing an *hpo* clone. The mutant clone is outlined by the dashed line.

(F) A high magnification view of epidermal cells near the border of an *hpo* clone on the notum. The dashed line marks the border between the wild-type cells and the mutant clone. The mutant clone is located to the right of the border.

(G) A *Drosophila* wing containing an *hpo* clone as outlined by the dashed line. Note the blister-like phenotype in the mutant clone.

(H) A portion of a *Drosophila* leg containing *hpo* mutant clones as outlined by the dashed lines.

(I) Section through an *hpo* clone in the adult eye. The mutant clone is marked by the absence of pigment. Note the increase in spacing between mutant photoreceptor clusters.

(J–J″) Third instar eye disc was stained with phalloidin (red), which highlights the outlines of the cells. hpo^- cells were marked by the lack of GFP signal (green). Three images are shown, one of GFP (J), one of phalloidin (J′), and one of superimposed GFP and phalloidin (J″). Supernumerary interommatidial cells are present in *hpo* clones.

(K–K″) and (L–L″): similar to (J–J″) except that the disc was stained for the neuronal specific Elav protein (K–K″) or R8 specific Senseless (Sens) protein (J–J″). Arrowhead marks the MF.

42–47, and *42–48*, define a single complementation, which was named *hippo* (*hpo*) based on the overgrowth phenotype in mosaic flies. All analyses in this report were performed using the null allele hpo^{42-47} (see below) unless otherwise indicated. Selective removal of *hpo* function in over 90% of the eye disc cells using the *eyeless*-FLP technique (Newsome et al., 2000) resulted in flies with enlarged, folded eyes and excess head cuticle (Figures 1A–1C). The external ommatidial facets were frequently lost (Figure 1C). *hpo* mutant clones induced in other tissues also resulted in overgrowth (Figures 1E–1H). In addition, the cuticle secreted by *hpo* mutant epidermal cells displays an unusual texture. In *hpo* mutant clones on the notum, the apical surface of the epidermal cells are clearly demarcated such that cell-cell boundaries are visible between adjacent cells, while cell boundaries are not visible in surrounding wild-type tissues (Figure 1F). A similar phenotype is seen in *hpo* mutant clones on the leg (Figure 1H) and the head cuticle (see Figure 8E). This phenotype most likely reflects abnormal morphology of the epidermal cells as shown previously for *wts* mutant cells (Justice et al., 1995).

Among our three *hpo* alleles, hpo^{42-47} elicited the most severe overgrowth, followed by hpo^{42-48}, with hpo^{42-20} being the weakest allele. For example, eyes composed predominantly of hpo^{42-20} cells have fewer folded eye tissues (Figure 1D), when compared to similar eyes composed of hpo^{42-47} cells (Figure 1C). The external ommatidial facets are also more evident in *eyeless*-FLP-hpo^{42-20} eyes (compare Figures 1D and 1C). The overgrowth phenotypes elicited by hpo^{42-47} are qualitatively similar to those previously described for mutations of the *Drosophila* tumor suppressor genes *sav* and *wts* (Xu et al., 1995; Justice et al., 1995; Tapon et al., 2002; Kango-Singh et al., 2002). Overall, the hpo^{42-47} phenotypes are more severe than those of null *sav* alleles but less severe than those of null *wts* alleles. This is also reflected by the different degrees of pupal lethality caused by removing *hpo*, *sav*, or *wts* function in the eye using the *eyeless*-FLP technique. While over 90% of *eyeless*-FLP-hpo^{42-20}

animals survive to adults, only 30% of *eyeless*-FLP-*hpo*$^{42–48}$ animals and 2% of *eyeless*-FLP-*hpo*$^{42–47}$ animals survive to adults. For comparison, nearly all *eyeless*-FLP-*sav*^{3} animals survive to adults, and none of *eyeless*-FLP-*wts*^{latsX1} animals survive to adults.

hpo Regulates Cell Proliferation

Sectioning of *hpo* mutant clones in adult eyes revealed a normal complement of photoreceptor cells (Figure 1I), suggesting that photoreceptor differentiation is not perturbed by loss of *hpo*. However, spacing between photoreceptor clusters is increased due to the presence of extra interommatidial cells (Figure 1I). These extra cells are pigment cells since they produced normal pigment when clones were induced in a w^{+} background (data not shown). The formation of extra interommatidial cells is evident in late-third instar eye discs, when *hpo* mutant clones at the posterior region of the eye imaginal disc contain many additional cells between photoreceptor clusters (Figures 1J–J″). To investigate whether the extra cells are due to abnormal ommatidial spacing and/or cell differentiation during early retinal patterning, we stained the eye imaginal discs for the neuronal marker Elav and the R8 marker Senseless (Sens). As seen in Figures 1K–1K″ and 1L–1L″, *hpo* mutant ommatidial clusters have the normal complement of differentiating photoreceptor cells (Figures 1K–1K″), and R8, the first photoreceptor cell to differentiate, is specified at correct location and density emerging from MF (Figures 1L–1L″). The spacing between adjacent ommatidial clusters is initially normal but increases at later stages, toward the posterior of the eye disc, due to the presence of extra interommatidial cells (Figures 1K–1K″ and 1L–1L″). Thus, in *hpo* mutant clones, early retina patterning is not affected, and photoreceptors exit cell cycle and differentiate normally. However, *hpo* mutant clones contain an increased number of uncommitted, interommatidial cells in third instar eye discs.

The increased number of interommatidial cells in *hpo* mutant clones could be due to increased cell proliferation, decreased apoptosis or a combination of both. To pinpoint the developmental cause of this phenotype, we first monitored cell proliferation in the eye imaginal discs. We used BrdU incorporation to label cells in the S phase. In wild-type eye discs, S phase cells are distributed randomly anterior to the MF. Cells are arrested synchronously in G1 within the MF and do not incorporate BrdU. Posterior to the MF, cells in the SMW (arrowhead in Figures 2A and 2A″) undergo a synchronous S phase that can be revealed as a band of BrdU-positive cells. Few BrdU-positive cells are found posterior to the SMW. In *hpo* mutant clones, uncommitted interommatidial cells fail to undergo cell cycle arrest posterior to the SMW, and continue S phase (Figures 2A and 2A″). At least some of these cells continue to proliferate during early pupal development, as revealed by ectopic BrdU incorporation (Figures 2B and 2B″) and the M phase marker phosphorylated histone H3 (PH3) (Figures 2C and 2C″) at 16 hr APF. *hpo* mutant cells in the compound eye eventually exit cell cycle and differentiate as pigment cells, and ectopic cell proliferation is undetectable beyond 24 hr APF (not shown).

To test whether *hpo* also affects the rate of cell multi-

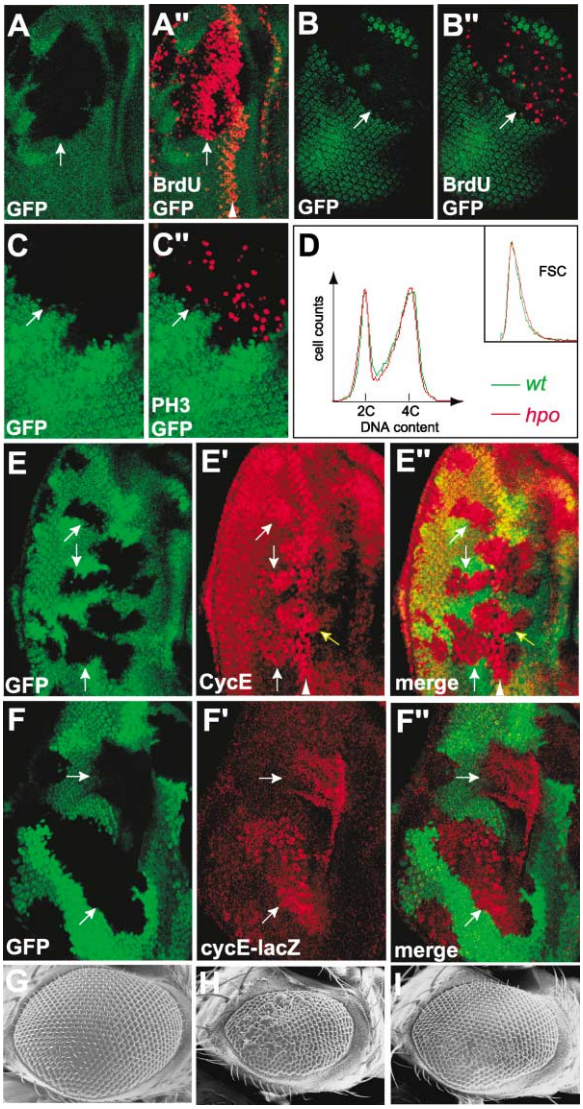

Figure 2. Cell Cycle Defects of *hpo* Mutant Cells

In all panels, *hpo* clones were marked by the absence of GFP signal (green) and indicated with arrows.

(A–A″) S phase was labeled by BrdU incorporation (red). Two images are shown, one of GFP (A) and one of superimposed GFP and BrdU staining (A″). While normally detected in a single band of cells in SMW (arrowhead), BrdU incorporation continues posterior to SMW in *hpo* mutant clones.

(B–B″) Similar to (A–A″) except that pupal eye disc was analyzed at 16 hr APF.

(C–C″) A 16 hr APF pupal eye stained for M phase marker phospho-H3 (PH3).

(D) Flow cytometric analysis of dissociated wing imaginal discs containing *hpo* mutant clones. The DNA profiles of *hpo* and wild-type cells are indicated by red and green traces, respectively. The insect shows forward scattering (FSC), which measures cell size.

(E–E″) A third instar eye disc stained with α-CycE (red), which normally reveals a band of intense staining in the SMW (arrowhead) and diminished expression posterior to the SMW. Note the elevated CycE staining posterior to the SMW in *hpo* mutant clones (arrows). Elevated CycE level was also seen in *hpo* mutant cells immediately anterior to the SMW (yellow arrow).

(F–F″) *hpo* mutant clones were generated in flies containing a *cycE-lacZ* reporter. The eye disc was stained for lacZ protein (red). Note the elevated level of cycE-lacZ in *hpo* clones.

(G–I) SEM images of compound eyes from wild-type (G), *cyE*^{JP}/*cycE*^{AR95} (H), and *cyE*^{JP} *hpo*$^{42-47}$/*cycE*$^{AR95+}$ (I).

plication during the growth phase of imaginal discs, we measured cell-doubling time for *hpo* mutant cells in the wing imaginal disc. The cell-doubling time for wild-type clones and *hpo* mutant clones (142 pairs of clones analyzed) was 13.9 hr and 12.2 hr, respectively. Thus, *hpo* mutant cells multiply faster in the wing discs. FACS analysis of dissociated wing disc cells showed that *hpo* mutant cells have a similar cell cycle profile and cell size (FSC) distribution as compared to wild-type cells (Figure 2D). Thus, loss of *hpo* does not accelerate a particular phase of the cell cycle during the growth period of imaginal discs. Rather, each phase of the cell cycle is proportionally accelerated.

A limiting factor for S phase entry in *Drosophila* imaginal discs is cyclin E (CycE) (Richardson et al., 1995; Neufeld et al., 1998). Thus, we examined CycE level in *hpo* mutant clones in the eye imaginal discs. Elevated CycE protein was detected in *hpo* mutant cells in the SMW and posterior to it (Figures 2E–2E″). Elevated CycE was also observed in *hpo* mutant cells just anterior to the SMW, although the effect was less profound (yellow arrow in Figure 2E–2E″). To investigate whether the regulation of CycE level by *hpo* is mediated by transcriptional or posttranscriptional mechanisms, we took advantage of a *cycE-lacZ* reporter that contains 16.4 kb of 5′ regulatory sequence of *cycE* (Duman-Scheel et al., 2002). Expression of the *cycE-lacZ* reporter was increased in *hpo* mutant clones, suggesting that the elevated level of CycE protein is mediated, at least in part, by an increase in *cycE* transcription. We further examined genetic interactions between *cycE* and *hpo*. $cycE^{JP}/cycE^{AR95}$ is an allelic combination that produces small and rough eye phenotype (Figure 2H). Both the roughness and eye size phenotype of this hypomorphic combination is dominantly suppressed by heterozygosity for *hpo* (Figure 2I). Thus, *cycE* is a critical downstream target of *hpo*.

hpo Regulates Apoptosis

Developmental apoptosis is most prominent in pupal retina around 36 hr APF when a wave apoptosis removes excessive interommatidial cells (Wolff and Ready, 1993). We assayed cell death using TUNEL or antibody against the activated caspase Drice (Yoo et al., 2002). Strikingly, in pupal eyes at 36 hr APF, cell death was suppressed in *hpo* mutant clones, even though abundant apoptosis was detected in the neighboring wild-type cells (Figures 3A–3A″ and 3B–3B″). Cell death in *hpo* mutant clones is not simply delayed, since we could not detect any significant cell death in *hpo* mutant clones up to 48 hr APF when the mature lattice of the retina is formed (data not shown). Thus, normal developmental apoptosis appears to require *hpo* function.

Consistent with the cell death defects, elevated level of DIAP1 protein was detected in *hpo* mutant clones in pupal eyes (Figures 3C–3C″) and third instar eye discs (Figures 3D–3D″). In third instar eye discs, elevated DIAP1 protein level is observed in all cells within the *hpo* mutant clones, irrespective of their differentiation status (Figures 3D–3D″). Thus, *hpo* acts cell autonomously to downregulate the level of DIAPI protein. To investigate whether the regulation of DIAPI is mediated by transcriptional or posttranscriptional mechanism, we used an enhancer trap insertion into the *diap1* locus

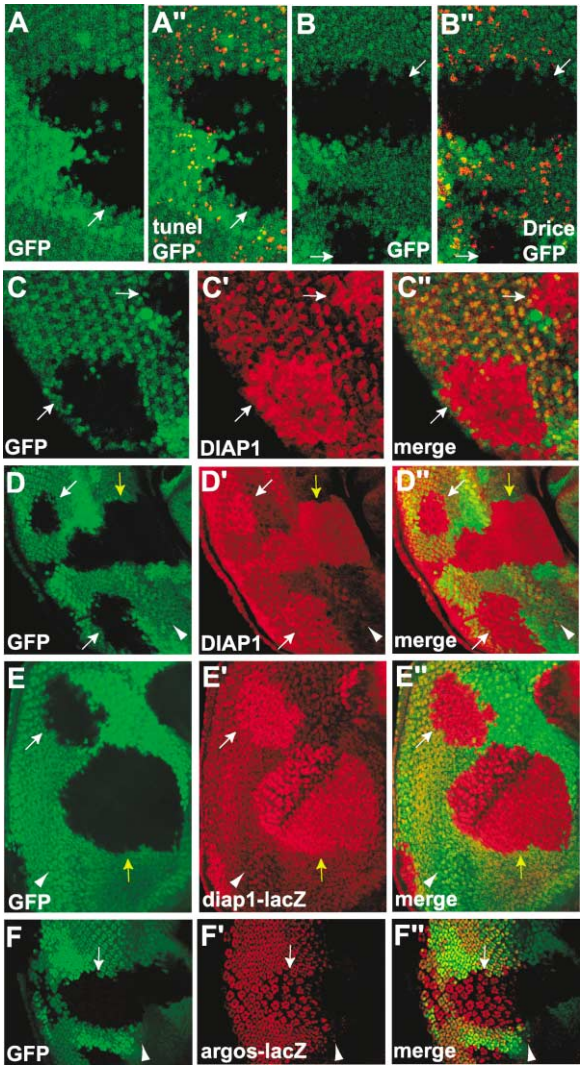

Figure 3. Cell Death Defects of *hpo* Mutant Cells

(A–A″) TUNEL staining (red) of a 36 hr APF pupal eye. Cell death is absent in *hpo* clones but abundant in the neighboring wild-type cells.

(B–B″) Similar to (A–A″) except that cell death was detected with α-active Drice. Arrows indicate two *hpo* clones. Note that cell death is largely confined to wild-type cells.

(C–C″) A 36 hr pupal eye stained with α-DIAP1 antibody (red).

(D–D″) Third instar eye disc stained with α-DIAP1 antibody (red). Arrowhead indicates MF. Note the elevated level of DIAP1 protein in *hpo* mutant cells irrespectively of their relative position to the MF. Yellow arrow indicates *hpo* mutant cells anterior to the MF.

(E–E″) Third instar eye disc containing th^{j5c8} and stained for lacZ protein (red). Arrowhead indicates MF. Note the elevated *diap1-lacZ* expression in *hpo* mutant cells irrespective of their relative position to the MF. Yellow arrow indicates *hpo* mutant cells anterior to the MF.

(F–F″) Third instar eye disc containing the $argos^{W11}$ *P[lacZ]* enhancer trap and stained for lacZ (red). Note the similar level of *argos-lacZ* expression in *hpo* and wild-type cells.

called th^{j5c8}. This enhancer trap line carries a *P[lacZ]* insertion in the 5′ untranslated region of *diap1* (Hay et al., 1995) and its expression pattern mimics that of endogenous *diap1*(Ryoo et al., 2002). Expression of the th^{j5c8} *P[lacZ]* reporter was elevated in *hpo* mutant clones in a cell-autonomous manner (Figures 3E–3E″). A similar increase in th^{j5c8} *P[lacZ]* reporter was also observed in

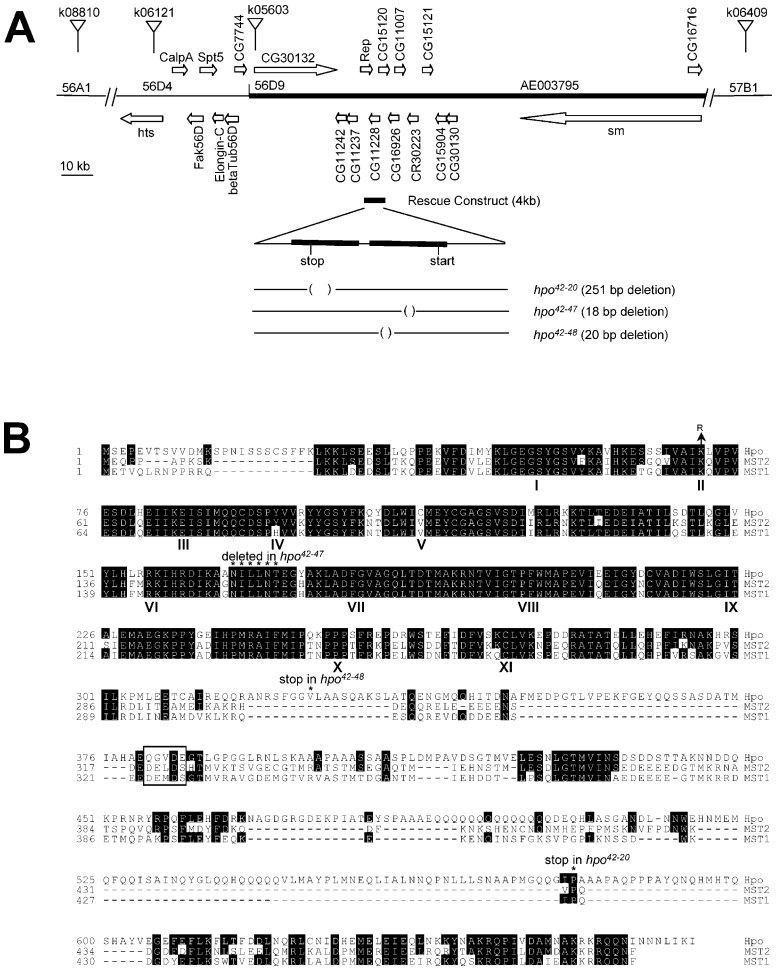

Figure 4. Identification of the *hpo* Gene

(A) Genomic organization of the 56A–57B region. P-elements used in the mapping of *hpo* are shown as triangles. The genomic DNA fragment used in the rescue construct is indicated. The translation start and stop sites of *hpo* are also marked.

(B) Sequence alignment of Hpo with MST2 and MST1. The 11 subdomains characteristic of protein kinases are indicated by Roman numerals. The C-terminal half of Hpo is less well conserved except for the last 60 amino acids. The K71R mutation that is used to generate kinase-dead Hpo is indicated. The boxed region represents the caspase cleavage site of MST1. Molecular lesions of hpo^{42-20}, hpo^{42-47}, and hpo^{42-48} are indicated.

hpo mutant clones in the wing discs (data not shown). The elevated level of *diap1-lacZ* is not due to increased stability of lacZ protein in *hpo* mutant cells, since expression of an unrelated *P[lacZ]* enhancer trap reporter was not affected in *hpo* mutant cells (Figures 3F–3F″). Quantification revealed that in *hpo* mutant cells, DIAP1 protein and *diap1-lacZ* reporter is 2.5 and 3.3-fold higher than that of wild-type cells, respectively. RT-PCR analysis confirmed an increase of *diap1* transcript level in *hpo* mutant cells (see Figure 5C). Thus, it appears that *hpo* regulates *diap1* largely through a transcriptional mechanism.

hpo Encodes a Ser/Thr Protein Kinase of the Ste-20 Family

Recombination mapping placed *hpo* between two P elements: *l(2)k08810* and *l(2)k06409* (Figure 4A). Male recombination mapping (Chen et al., 1998) further localized *hpo* distal to *l(2)k06121* and *l(2)k05603* (Figure 4A). These two P elements were also used for meiotic mapping. While one recombinant between *hpo* and *l(2)k06121* was recovered from 500 events, none was recovered between *hpo* and *l(2)k05603*. These results suggest that *hpo* lies distal but close to *l(2)k05603*. Starting from the insertion site of *l(2)k05603*, a series of contiguous DNA fragments were used to probe genomic DNA blots prepared from all *hpo* alleles. One fragment 40 kb away from *l(2)k05603* revealed a polymorphism associated with hpo^{42-20}. Sequencing analysis revealed that hpo^{42-20} contains a 251 bp deletion in the CG11228 gene. Analysis of genomic DNA from the remaining two *hpo* alleles revealed an 18 bp deletion in hpo^{42-47} and 20 bp deletion in hpo^{42-48} in the predicted coding exons of CG11228 (Figure 4A), suggesting that CG11228 corresponds to *hpo*. We have thus renamed CG11228 as *hpo*.

hpo encodes a polypeptide with an N-terminal kinase domain and a noncatalytic C-terminal domain (Figure 4B). Its kinase domain reveals Hpo as a member of the Ste20 family Ser/Thr kinases. The founding member of this family, Ste20, is a putative yeast mitogen-activated protein kinase kinase kinase kinase (MAP4K) involved in the mating pathways. The Ste20 family kinases are further divided into the p21-activated kinases (PAK) and germinal center kinase (GCK) subfamilies. The overall architecture and catalytic domain sequence further places Hpo into the group II GCK (Dan et al., 2001). Hpo is most closely related to human proteins MST2 (60% identity) and MST1 (58% identity). MST1 and MST2 were first isolated based on their homology to yeast Ste20 (Creasy and Chernoff, 1995) and independently identified as kinases activated in NIH3T3 cells by extreme stress (Taylor et al., 1996). Little is known about the

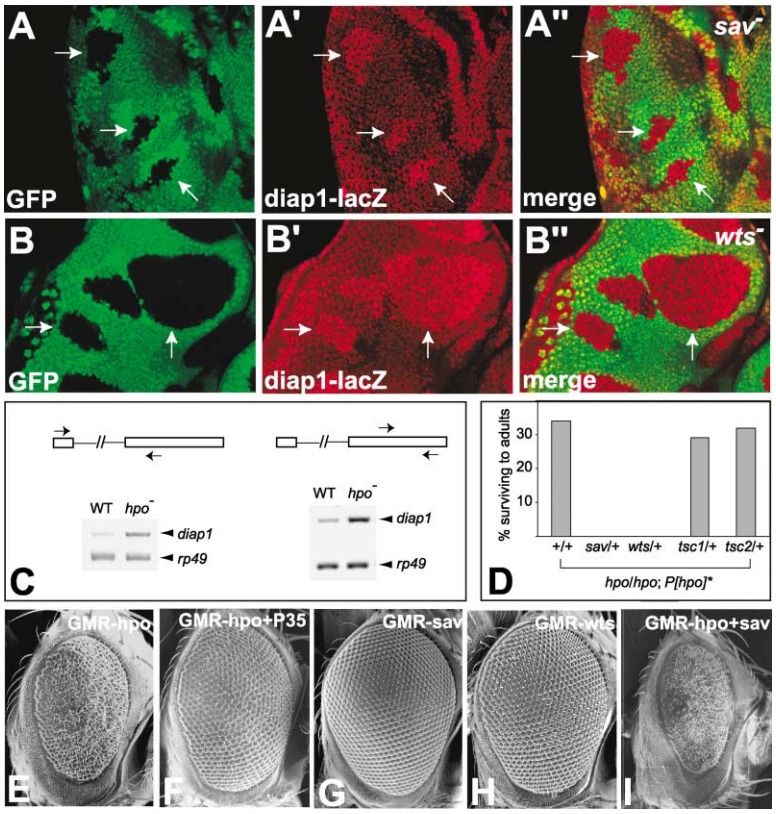

Figure 5. Genetic Interactions among *hpo*, *sav*, and *wts*

(A–A″) sav^{3} clones were analyzed in third instar eye discs carrying th^{j5c8}. Note the elevated *diap1-lacZ* expression (red) in *sav* clones. Similar results were seen in sav^{4} clones (not shown).

(B–B″) Similar to (A–A″) except that wts^{latsX1} mutant clones were analyzed. Note the elevated *diap1-lacZ* expression in *wts* clones.

(C) RT-PCR analysis of total RNA extracted from control and hpo^{42-47} first instar larvae. The diagram shows the major splicing form of the *diap1* gene (Hay et al., 1995). th^{j5c8} carries *P[lacZ]* insertion in the first (noncoding) exon (Hay et al., 1995). Also shown on the diagrams are *diap1* primers (arrows) used in RT-PCR, with one set of primers spanning the intron (left gel) and the other set located within the second (coding) exon (right gel). Primers corresponding to *rp49* gene are used as internal controls for RT-PCR.

(D) Dosage sensitive genetic interactions between *hpo*, *sav*, and *wts*. Heterozygous mutations of *sav*, *wts*, *Tsc1*, and *Tsc2* were introduced into a hypomorphic *hpo* mutant background (see text for details). The percentage of flies surviving to adults is shown for various genotypes. The *sav* alleles used were sav^{3} and sav^{4}. The *wts* alleles used were wts^{latsX1} and *Df(3R)tll-g*.

(E–I) SEM images of compound eyes from the following genotype: *GMR-hpo* (E), *GMR-P35*; *GMR-hpo* (F); *GMR-sav* (G), *GMR-wts* (H), and *GMR-hpo; and GMR-sav* (I).

physiological function of MST2; however, several reports have shown that overexpression of MST1 promotes apoptosis and that MST1 itself is cleaved by caspases during apoptosis (Graves et al., 1998). Interestingly, the identified caspase cleavage site of MST1 ($DEMD^{326}S$, see Figure 4B) is not conserved in Hpo. In particular, Hpo contains glutamate instead of serine immediately C-terminal to the putative caspase cleavage (Figure 4B), and a S327E mutation of MST1 completely abolishes its cleavage by caspases (Glantschnig et al., 2002). Thus, the *Drosophila* Hpo kinase is an improbable caspase substrate.

The molecular defects of the *hpo* alleles correlate with their overgrowth phenotype. hpo^{42-47} causes an in-frame deletion of 6 residues ($N^{166}ILLNT^{171}$) in kinase subdomain VI. N^{166} is involved in ATP binding, and is one of the nine residues that are identical in all kinases (Hanks et al., 1988). Thus, hpo^{42-47} is predicted a null allele. On the other hand, hpo^{42-48} is predicted to delete most of the C-terminal noncatalytic domain of the Hpo, while hpo^{42-20} deletes the last 91 residues at the C terminus of Hpo. Thus, hpo^{42-20} and hpo^{42-48} are expected to be weaker alleles than hpo^{42-47}, a prediction that agrees with the phenotypic analyses of the *hpo* allelic series. A construct containing only the CG11228 locus was tested for its ability to rescue *hpo* mutant flies (Figure 4A). Nine out of ten independent transgenic lines tested fully rescued hpo^{42-20}, hpo^{42-47}, or hpo^{42-48} homozygotes to wild-type adults, further confirming that *hpo* corresponds to CG11228. The remaining line, *P[hpo]**, failed to rescue the lethality of hpo^{42-47} or hpo^{42-48}, but partially rescued the lethality of hpo^{42-20}. 34% of hpo^{42-20} homozygotes carrying a copy of *P[hpo]** survived to adults with phenotypes such as held-out wings and mild overgrowth. As described later, this partially rescued genetic combination provides a sensitized genetic background to examine interactions with other components of the *hpo* pathway.

Genetic Interaction among *hpo*, *sav*, and *wts*

The cell cycle and apoptosis defects associated with *hpo* are similar to those described for *sav* and *wts*, including elevated *cycE* transcription, increased cell proliferation, and decreased cell death (Tapon et al., 2002). However, our results differ significantly from the report of Tapon et al. (2002) regarding the mechanisms of DIAP1 regulation by *sav*. While we observed a clear upregulation of *diap1* transcription in *hpo* mutant cells, it was reported that *diap1* transcription is not affected in *sav* mutant cells. *wts* mutant clones were not analyzed in the previous report (Tapon et al., 2002). This discrepancy prompted us to reevaluate *sav* mutant clones using the th^{j5c8} enhancer trap as a readout for *diap1* transcription. As shown in Figures 5A–5A″, loss of *sav* clearly leads to upregulation of *diap1* transcription. Tapon et al. (2002) used whole mount in situ hybridization to detect *diap1* transcript without marking mutant clones, thus preventing a careful comparison of *diap1* transcripts at high resolution. We further examined mutant clones of *wts* using the th^{j5c8} *P[lacZ]* reporter and observed a similar increase in *diap1* transcription (Figures 5B–5B″). RT-PCR analysis revealed an increase in *diap1* mRNA in

hpo mutant larvae as compared to wild-type controls (Figure 5C). Taken together, these data suggest that *hpo*, *sav*, and *wts* likely function in a common signaling pathway that coordinately controls cell proliferation and apoptosis, at least partly through regulation of *cycE* and *diap1* transcription.

To further probe the link between *hpo*, *sav*, and *wts*, we investigated their genetic interactions. As described earlier, hpo^{42-20} homozygotes carrying a copy of *P[hpo]** represents a sensitized genetic background in which *hpo* activity is compromised to a level that allows only a fraction of the animals to survive to adulthood. We observed a dramatic genetic interaction between *hpo* and *sav* or *wts* in this genetic background. While 34% of hpo^{42-20} homozygotes carrying a copy of *P[hpo]** survive to adults, none of them survive to adulthood if these animals are simultaneously heterozygous for *sav* or *wts* (Figure 5D). No genetic interactions were observed between *hpo* and tumor suppressor genes *Tsc1* and *Tsc2* (Figure 5D).

To complement the above genetic analyses, we created a gain-of-function genetic background for *hpo* and used it to examine genetic interactions between *hpo*, *sav*, and *wts*. Overexpression of *hpo* using the GMR promoter results in a rough eye phenotype (Figure 5E), which is largely suppressed by coexpression of cell death inhibitor P35 (Figure 5F). As described previously, overexpression of *sav* by the GMR promoter has no effect (Figure 5G), while overexpression of *wts* by the GMR promoter generates very subtle irregularities in ommatidial arrangement (Figure 5H) (Tapon et al., 2002). Interestingly, coexpression of *hpo* and *sav* by the GMR promoter results in greatly reduced eye size (Figure 5I), and coexpression of *hpo* and *wts* by the GMR promoter results in 100% lethality at early pupal stage. These genetic interactions further implicate *hpo*, *sav*, and *wts* in a common signaling pathway.

Hpo Associates with and Phosphorylates Sav

We carried out a yeast two-hybrid screen in the hope of identifying Hpo binding proteins. We screened approximately 1 million cDNA clones using as bait the noncatalytic C-terminal portion of Hpo (Figure 6A). Interestingly, 6 out of 12 positive clones isolated from the screen corresponded to Sav, representing 3 different classes of clones (Figure 6A). These Hpo-interacting Sav clones define the C-terminal half of Sav (residues 362–607) as an Hpo binding region. This region contains predicted Sav WW and coiled-coil domains (Tapon et al., 2002; Kango-Singh et al., 2002). We carried out another yeast two-hybrid screen using the C-terminal half of Sav as the bait (Figure 6A). In this screen, 5 out of 45 positive clones isolated from the screen corresponded to Hpo, representing 4 different classes of clones (Figure 6A). These Sav-interacting Hpo clones define the C-terminal portion of Hpo (residues 474–669) as a Sav binding region. The identification of Hpo and Sav as interacting proteins in unbiased yeast two-hybrid screens provides strong evidence that these proteins interact with each other in vivo. Consistent with this hypothesis, Hpo and Sav associate with each other in vitro. As shown in Figure 6B, GST fusion protein containing full-length Sav, but not a control GST fusion protein, was able to specifically pull-down endogenous Hpo protein from S2 cell extracts. Hpo and Sav also interact with each other in coimmunoprecipitation assays (see Figure 7F).

We next investigated whether Hpo could function as a Sav kinase. For this purpose, we established a cotransfection assay in S2 cells. As shown in Figure 6C, coexpression of Hpo and Sav resulted in retarded mobility of Sav (compare lanes 1 and 3), leading to the formation of multiple slower migrating bands. Phosphatase treatment abrogated this shift (Figure 6D), suggesting that the mobility shift is due to protein phosphorylation. On the other hand, coexpression of Sav and Wts, also a Ser/Thr kinase, did not result in Sav mobility shift (compare lanes 1 and 2), nor did expression of Wts affect the phosphorylation of Sav by Hpo (compare lanes 3 and 4). In vitro, myc-tagged Hpo protein specifically phosphorylated a GST fusion protein containing the Hpo binding region of Sav (lane 2 in Figure 6E), while no signals were detected using a control substrate or the kinase dead Hpo^{K71R} mutant (lanes 1 and 3 of Figure 6E). Thus, Hpo phosphorylates Sav.

The results presented above suggest a model wherein the C-terminal domain of Hpo associates with Sav and presents Sav to the Hpo kinase. If so, a kinase-dead mutant of Hpo, or the C-terminal noncatalytic domain of Hpo expressed alone, should behave as dominant-negative forms, since these variants should associate nonproductively with endogenous Sav and interfere with signal propagation. Indeed this is the case. While expression of wild-type Hpo using the wing-specific *MS1096* Gal4 driver results in a dramatically reduced wing size (Figures 6F and 6G), expression of the kinase dead Hpo^{K71R} mutant results in 35% increase in wing size (Figures 6F and 6H). Similarly, an increase (31%) in wing size is observed upon expression of $Hpo^{318-669}$, which contains just the C-terminal noncatalytic domain of Hpo (Figures 6F and 6I).

Hpo/Sav Interaction Promotes Wts Phosphorylation

Having established a functional link between Hpo and Sav and given the results from our genetic analyses implicating *hpo*, *sav*, and *wts* in a common pathway, we investigated whether Wts might be regulated by Hpo and/or Sav. In S2 cells, expression of Hpo results in retarded mobility of Wts, while coexpression of Hpo and Sav results in a further mobility shift of Wts (Figure 7A). For simplicity, we refer to this further shift of Wts upon coexpression of Hpo and Sav as "supershift" to be distinguished from the mobility shift caused by expression of Hpo alone. Both shifts were largely abolished by phosphatase treatment, confirming that the shifts were due to phosphorylation (Figure 7B). Taken together, these data suggest that Sav increases the ability of Hpo to phosphorylate Wts.

The mobility shift assay described above allowed us to narrow down the domain of Wts that is the target of Hpo-mediated phosphorylation to a region at the N-terminal noncatalytic portion (residues 68–414) of the Wts protein (Figure 7C). In vitro, a GST fusion protein containing this region of Wts was phosphorylated by Hpo, while no signals were detected using a control substrate or the kinase dead Hpo^{K71R} (Figure 7D). Consis-

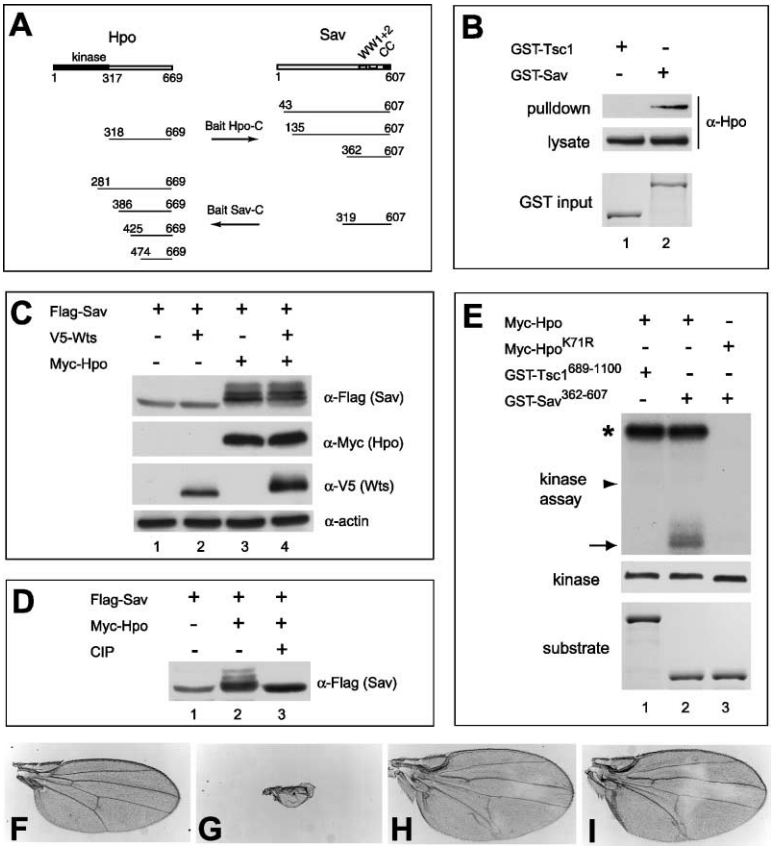

Figure 6. Hpo Binds to and Phosphorylates Sav

(A) Unbiased yeast two-hybrid screens identify Hpo and Sav as interacting proteins. The schematic structures of Hpo and Sav proteins are shown at the top. "WW1+2" and "CC" refer to the two WW domains and the coiled-coil domain of Sav. Schematics of the bait and the interacting preys from each screen are shown.

(B) Association between Hpo and Sav in vitro. S2 cell lysates were incubated with glutathione Sepharose beads containing GST-Sav or GST-Tsc1 (as a control). Endogenous Hpo protein present in the cell lysates (lysate) or associated with the beads (pull-down) was probed with α-Hpo antibody.

(C) Hpo, but not Wts, stimulates the phosphorylation of Sav in S2 cells. Lysates from S2 cells expressing various epitope-tagged proteins were probed with indicated antibodies. Expression of Hpo, but not Wts, results in mobility shift of the coexpressed Sav protein (lanes 1–3).

(D) Phosphatase (CIP) treatment reversed the mobility shift of Sav induced by Hpo.

(E) Hpo phosphorylates Sav in vitro. Myc-tagged Hpo or Hpo^{K71R} was immunoprecipitated from S2 cells and tested for kinase activity against GST-Sav$^{362-607}$ and GST-Tsc1 (as a control substrate). The signal of GST-Sav phosphorylation by Hpo is indicated by an arrow. The arrowhead marks the expected migration position of the GST-Tsc1 and the asterisk indicates signals resulting from Hpo autophosphorylation. The input kinase and substrate are also shown (bottom two gels).

(F–I) Kinase-dead Hpo or C-terminal noncatalytic domain of Hpo behave in a dominant-negative manner. *Drosophila* wings from the following genotypes are shown: *MS1096*; + (F), *MS1096*; *UAS-hpo* (G), *MS1096*; *UAS-hpo*^{K71R} (H) and *MS1096*; and *UAS-hpo*$^{318-669}$ (I).

tent with Wts as a kinase substrate of Hpo, the mobility of endogenous Wts protein on SDS-PAGE is increased in Hpo mutant animals (Figure 7E).

Our results suggest a model wherein Hpo associates with and phosphorylates Sav and interactions between Hpo and Sav facilitate Wts phosphorylation by Hpo. This model is consistent with previous report of direct physical interaction between Sav and Wts (Tapon et al., 2002). Thus, Sav could be viewed as an adaptor protein that brings Hpo in proximity to Wts to facilitate Wts phosphorylation. Since the Sav WW domains have been implicated in Sav/Wts interaction (Tapon et al., 2002), we speculated that the coiled-coil domain of Sav, located C-terminal to the WW domains, might be involved in Sav/Hpo interaction (see Figure 6A for schematics of Sav domains). Interestingly, the *shrp6* allele of *sav* causes a frameshift mutation that truncates just the coiled-coil domain but leaves the WW domains intact (Kango-Singh et al., 2002). To pinpoint the functional defect of the *sav*^{shrp6} allele, we engineered a mutant Sav protein, Sav^{shrp6}, that lacks the C-terminal 79 residues as seen in *sav*^{shrp6}, and examined the ability of this mutant protein to associate with Hpo and to facilitate Wts phosphorylation by Hpo. Unlike wild-type Sav, Sav^{shrp6} could not associate with Hpo (Figure 7F), suggesting that the coiled-coil domain of Sav is required for Hpo/Sav interaction. Importantly, coexpression of Sav^{shrp6} and Hpo could no longer cause the supershift of Wts as seen when wild-type Sav and Hpo are coexpressed (Figure 7G). Thus, Hpo/Sav interaction is required for Sav to facilitate the phosphorylation of Wts by Hpo.

A Human Homolog of *hpo* Rescues the Overgrowth Phenotype of *Drosophila hpo* Mutants

Hpo encodes a Ste-20 family protein kinase whose closest relative in humans is MST2 (60% identity). To test the functional significance of the sequence conservation between Hpo and MST2 and to gain insights into the function of MST2, we tested whether the overgrowth phenotype of *Drosophila hpo* mutant tissues could be rescued by expression of human *MST2*. We introduced *MST2* cDNA into *Drosophila* under the control of the *hsp70* promoter. A 60 min heat shock pulse per day starting from the 2nd instar larval stage until eclosion completely suppressed the overgrown-head phenotype associated *eyeless*-FLP-*hpo*$^{42-47}$ (Figures 8A–8D). The abnormal cell morphology phenotype was also completely rescued (compare Figures 8E and 8F). Taken together, these results reveal a high degree of functional conservation between Hpo and MST2 and raise the intriguing possibility that MST2 might play a similar role in mammalian growth control.

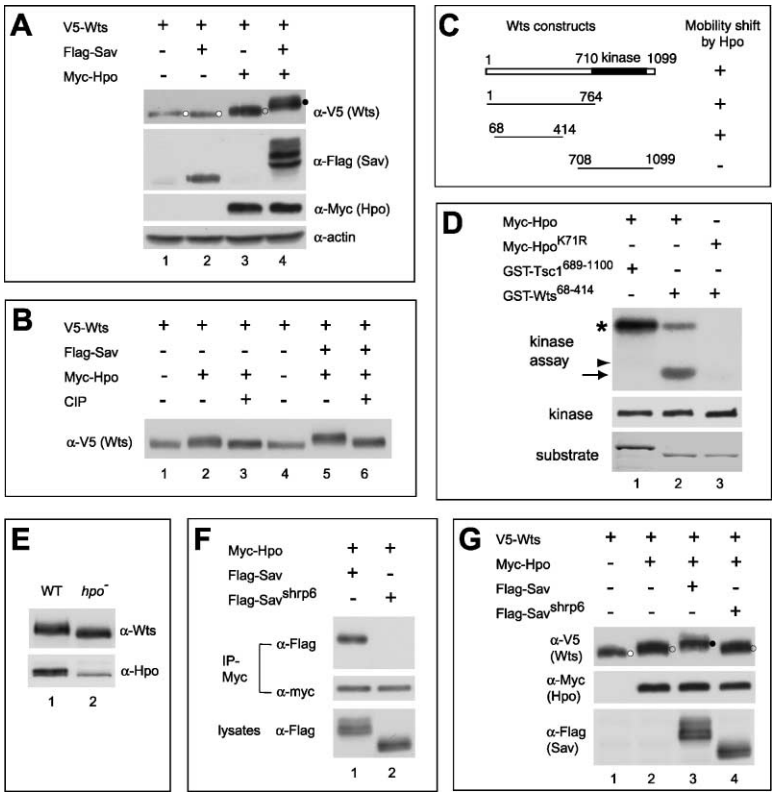

Figure 7. Hpo/Sav Interaction Promotes Wts Phosphorylation

(A) Sav facilitates the phosphorylation of Wts by Hpo. Expression of Hpo, but not Sav, results in a mobility shift of the coexpressed Wts protein (compare lanes 2 and 3). Also note the supershift of Wts when both Sav and Hpo are expressed (compare lanes 3 and 4). Increasingly phosphorylated forms of Wts are indicated by small circles next to the protein bands, and filled with white, gray, and black colors respectively.

(B) Phosphatase (CIP) treatment reversed the mobility shift of Wts induced by Hpo.

(C) Deletion mapping of the region of Wts phosphorylated by Hpo. The indicated Wts constructs were cotransfected into S2 cells with Hpo- and Sav-expressing plasmids.

(D) Hpo phosphorylates Wts in vitro. Myc-tagged Hpo or Hpo^{K71R} was immunoprecipitated from S2 cells and tested for kinase activity against GST-Wts$^{68–414}$ and GST-Tsc1. The signal of GST-Wts phosphorylation by Hpo is indicated by an arrow. The arrowhead marks the expected migration position of GST-Tsc1and the asterisk indicates signals resulting from Hpo autophosphorylation. The input kinase and substrate are also shown (bottom two gels).

(E) Hpo is required for Wts phosphorylation in vivo. Protein extracts from wild-type and *hpo*$^{42–47}$ 1st instar larvae were probed with antibodies against Wts and Hpo. Note the increased mobility of Wts from *hpo*$^{-}$ animals. Also note that Hpo appears as doublet in wild-type extracts due to autophosphorylation, but migrates as a single band in *hpo*$^{42–47}$, which produces a kinase-dead form of Hpo.

(F) Association between Hpo and wild-type Sav or Sav^{shrp6} was examined by coimmunoprecipitation. Wild-type Sav, but not Sav^{shrp6}, was detected in Myc-Hpo immunoprecipitates.

(G) The coiled-coil domain of Sav is required for Sav to promote Wts phosphorylation by Hpo. Note that the supershift of Wts is observed when wild-type Sav (lane 3), but not Sav^{shrp6} (lane 4), was expressed with Hpo. Increasingly phosphorylated forms of Wts are indicated by small circles next to the protein bands, and filled with white, gray, and black colors, respectively.

Discussion

The mechanisms of how body and organ size are regulated are largely unknown (Conlon and Raff, 1999). The final size of an organ or organism is a function of both cell size and cell number. Thus, size control in animal development is likely to involve a complex interplay of cell growth, proliferation, and death. Recent studies in *Drosophila* have implicated a number of pathways in the control of cell growth and proliferation, including the Ras and Myc oncogenes, cyclin D/cdk4, insulin/PI3K, and TSC/TOR pathways (Stocker and Hafen, 2000; Johnston and Gallant, 2002). Less is known about the contribution of cell death to developmental size control in *Drosophila*. Expression of P35 effectively blocks apoptosis in *Drosophila* but has no detectable effects on the growth of imaginal disc cells (Neufeld et al., 1998), suggesting that blocking cell death alone is not sufficient to offset the "mass checkpoint" that dictates the final size of imaginal discs. One possibility is that reduced apoptosis is compensated by decreased cell proliferation. Thus, decreased cell death might have to be coupled with a concomitant increase in cell proliferation in order to offset the mass checkpoint. This hypothesis is supported by studies of *sav*, a tumor suppressor gene that negatively regulates CycE and DIAP1 levels (Tapon et al., 2002), and *bantam*, a microRNA that promotes cell proliferation as well as downregulates the proapoptotic gene *hid* (Brennecke et al., 2003). Such coupling between cell death and proliferation is also likely an important element in cancer. Indeed, it is believed that deregulated proliferation together with suppressed apoptosis forms an obligate and perhaps universal platform to support neoplastic progression (Green and Evan, 2002).

In this report, we provide evidence that *hpo* represents an essential regulator of organ size through its dual roles in cell proliferation and apoptosis. Loss of *hpo* does not affect cell fate but leads to increased cell proliferation and decreased apoptosis. A critical downstream effector of *hpo* in cell proliferation is *cycE*, whose transcription level is increased in *hpo* mutant cells. That *cycE* represents a critical downstream effector of *hpo* is consistent with previous studies implicating the CycE/cdk2 complex as a central regulator of cell cycle progression in *Drosophila* (Richardson et al., 1995; Neufeld et al., 1998). Our analyses further identify the cell death inhibitor *diap1* as another downstream effector of *hpo*. In *Drosophila*, cell death molecules such as Reaper, Hid, and Grim downregulate DIAP1 activity through several post-transcriptional mechanisms, including direct binding,

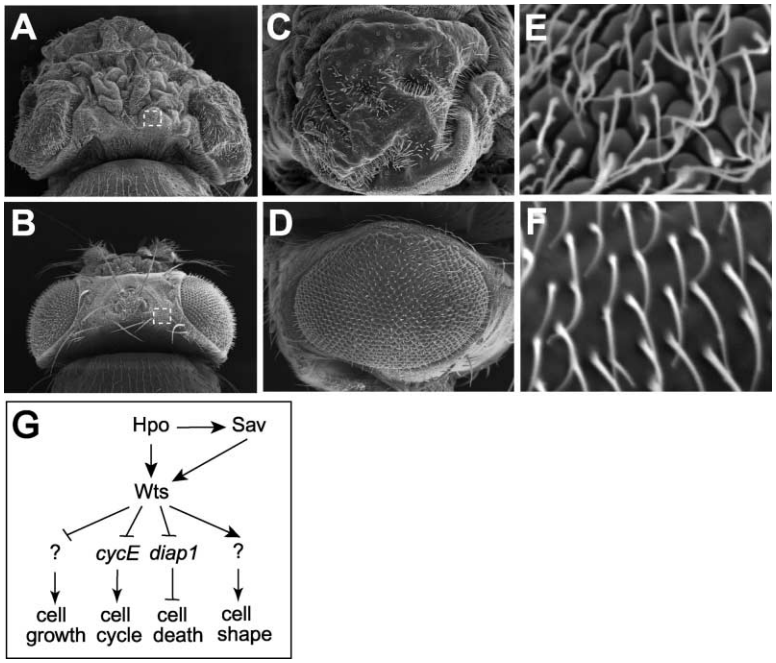

Figure 8. A Human Homolog of *hpo* Rescues the Overgrowth Phenotype of *Drosophila hpo* Mutants

(A–B) Dorsal view of *Drosophila* heads in which *hpo* function was selectively removed in the eye-antennal disc, in the absence (A) or presence (B) of the *hsp70-MST2* transgene expression. The genotypes are (A) *y w ey-flp*; hpo^{42-47} *FRT42D/FRT42D* w^+ *l(2)c1-R11* and (B) *y w ey-flp*; hpo^{42-47} *FRT42D/FRT42D* w^+ *l(2)c1-R11*; *P[hsp70-MST2]*. Both flies were treated by one 60 min heat shock (at 38°C) per day starting from the second instar larval stage until eclosion. Note the highly folded head cuticles and eye tissues in (A), which were completely suppressed by expression of *MST2* (B). The boxed areas in (A–B) are shown at higher magnification in (E–F).

(C-D) Similar to (A–B) except that SEM images of compound eyes instead of the heads are shown. *hsp70-MST2* was absent in (C), but present in (D). Note the highly disorganized eye structure in (C) and the near wild-type appearance of the compound eye in (D).

(E-F) High magnification view of the boxed areas in (A–B), showing detailed morphology of head cuticles. *hsp70-MST2* was absent in (E), but present in (F). Note the distinct cell-cell boundaries and the honeycomb-like appearance of the mutant epidermal cells (E), which was not seen in animals expressing *MST2*.

(G) A tentative model of the Hpo-Sav-Wts pathway in size control. Hpo associates with and phosphorylates Sav. Hpo/Sav interaction promotes the phosphorylation of Wts by Hpo. Potential downstream effectors of the pathway are also illustrated.

DIAP1 ubiquitination, or a general inhibition of protein translation (reviewed in Martin, 2002). Unlike Reaper, Hid, or Grim, Hpo appears to regulate DIAP1 largely through a transcriptional mechanism. To our knowledge, such a mode of DIAP1 regulation has not been described previously in *Drosophila*. Our studies also raise the intriguing possibility that jointly elevated CycE and IAP levels might represent a common pathway for tumor progression in humans.

While a great deal is yet to be learned about the mechanism of Hpo function in growth suppression, here we provide genetic and biochemical evidence that Sav and Wts are additional components of this emerging pathway (Figure 8G). Hpo encodes a Ste-20 family Ser/Thr kinase that associates with and phosphorylates Sav. The Hpo/Sav interaction promotes the phosphorylation of Wts by Hpo. The biochemical interactions among Hpo, Sav, and Wts are supported by the dosage-sensitive genetic interactions among these genes and the comparable upregulation of *cycE* and *diap1* transcription in each of their mutant backgrounds. Our model might explain why loss of *wts* results in the greatest overgrowth among the three genes, since it is the most downstream component among the three. Loss of *wts* might be expected to completely abolish the output of this pathway, while loss of *hpo* or *sav* might still leave Wts with some level of kinase activity. Our model might also explain why *sav* mutations result in the least severe phenotype among the three, since Sav facilitates, but is not absolutely required for, the phosphorylation of Wts by Hpo. Besides *cycE* and *diap1*, additional effectors downstream of the Hpo pathway are likely to exist. The cell morphology phenotype, for example, is likely mediated by some unknown target(s) of this pathway. Indeed, protein kinases related to Wts have been implicated in cytoskeleton and cell shape regulation in *S. pombe*, Neurospora, and *C. elegans* (Zallen et al., 2000 and references therein). In addition, there likely exist effector(s) of the Hpo pathway in cell growth, since cell growth must be proportionally stimulated to sustain the increased proliferation of *hpo*, *sav*, or *wts* mutant cells.

We propose that Hpo, Sav, and Wts define a tumor suppression pathway that coordinately regulates cell proliferation and apoptosis, and the Hpo-Sav-Wts pathway might be involved in tumorigenesis in mammals. Indeed, mice lacking a *wts* ortholog develop soft-tissue sarcomas and ovarian tumors (St John et al., 1999), and a human ortholog of *wts* is downregulated in a subset of soft-tissue sarcomas (Hisaoka et al., 2002). In addition, the human ortholog of *sav* is mutated in several cancer cell lines (Tapon et al., 2002). While we have not directly examined the role of *hpo* in human cancers, we show here that MST2, a human homolog of Hpo, completely rescues flies lacking *hpo*, revealing a high degree of functional conservation between flies and humans. It will be important to identify upstream regulators of the Hpo pathway, which might provide critical insights into the nature of the signal(s) that normally stop growth when a given organ reaches its characteristic size. The conservation of Hpo, Sav, and Wts from *Drosophila* to humans suggest that such size-control mechanisms are likely universal to all animals.

Experimental Procedures

Drosophila Genetics

All crosses and staging were done at 25°C. Null alleles of *sav* and *wts*, including sav^3, sav^4, and wts^{latsX1}, as well as *GMR-wts* and *GMR-sav* lines were kindly provided by Iswar Hariharan. th^{i5c8} and *cycE-lacZ* were gifts of Hermann Steller and Wei Du, respectively. cyE^{JP} and $cycE^{AR95}$ were gifts from Helena Richardson and Christian

Lehner, respectively. *Tsc1*^{29} and *Tsc2*^{192} alleles were described previously (Gao and Pan, 2001).

Molecular Biology and Yeast Two-Hybrid Screens

Genomic DNA was isolated from *hpo* mutant embryos and amplified with PCR. The PCR products were directly sequenced using primers spanning the *hpo* locus. A 4.0 kb genomic fragment containing just the *hpo* transcription unit was cloned into Casperhs-1, a modified Casperhs vector (Pan and Rubin, 1997), for the rescue experiment. A full-length *hpo* cDNA clone, GH10354, was obtained from Research Genetics and used to generate UAS and GMR constructs. The *MST2* cDNA was obtained from Research Genetics and cloned into the pCasper-hs vector to generate *hsp70-MST2*.

Myc-tagged Hpo, Flag-tagged Sav, and V5/His-tagged Wts constructs were made using the pAc5.1/V5-HisB vector (Invitrogen). Sequences encoding the N-terminal Myc epitope (MEQKLISEEDLNE) or Flag epitope (MDYKDDDDK) was added by PCR in place of the first Met codon of the respective cDNA clones.

Yeast two-hybrid screens were carried out using Stratagene's CytoTrap system and *Drosophila* cDNA library according to manufacturer's instructions.

Cell Transfection, Immunoprecipitation, GST Pull-Down and In Vitro Kinase Assays

Transfection and immunoprecipitation in S2 cells were carried out as described previously (Gao and Pan, 2001). GST pull-down assay was carried out as described (Tapon et al., 2002). For in vitro kinase assay, S2 cells expressing myc-tagged Hpo or Hpo^{K71R} were lysed in lysis buffer containing 50 mM HEPES [pH 7.4], 50 mM NaCl, 1 mM EDTA, 0.5% NP-40 plus phosphatase and protease inhibitors cocktail. Hpo was immunoprecipitated with anti-myc antibody and protein G-Sepharose. Immunoprecipitates were washed and incubated with recombinant substrate GST fusion proteins in kinase buffer containing 40 mM HEPES [pH 7.4], 10 mM MgCl2, 10 μM ATP, and 10 μCi/ml γ-P^{32}ATP at 30°C for 45 min.

Histology and Cell Cycle Analysis

Antibodies against Sens, CycE were gifts from Hugo Bellen and Terry Orr-Weaver, respectively. Antibodies against Drice and DIAP1 were gifts from Bruce Hay.

FACS analysis of dissociated imaginal wing disc cells was performed as described (Neufeld et al., 1998) using FACStar machine and analyzed with CellQuest program. Cell doubling time analysis was carried out as described (Neufeld et al., 1998) using *hpo*$^{42-47}$ mutant clones induced at 48 hr AED and analyzed at 120 hr AED. Cell doubling times were derived using the formula (log 2/log N)hr, where N = median number of cells/clone and hr = time between heat shock and disc fixation.

Acknowledgments

We apologize for deleting several references due to space limitation. We would like to thank Bruce Edgar and Keith Wharton for critical reading of the manuscript, and Hugo Bellen, Wei Du, Iswar Hariharan, Bruce Hay, Christian Lehner, Terry Orr-Weaver, Helena Richardson, and Hermann Steller for various reagents. D.J.P. is a Virginia Murchison Linthicum Endowed Scholar in Medical Science and is supported by grants from NIH (GM62323), American Heart Association (0130222N), and American Cancer Society (RSG0303601DDC).

Received: May 22, 2003
Revised: June 23, 2003
Accepted: June 23, 2003
Published online: July 15, 2003

References

Brennecke, J., Hipfner, D.R., Stark, A., Russell, R.B., and Cohen, S.M. (2003). bantam encodes a developmentally regulated microRNA that controls cell proliferation and regulates the proapoptotic gene hid in *Drosophila*. Cell *113*, 25–36.

Chen, B., Chu, T., Harms, E., Gergen, J.P., and Strickland, S. (1998). Mapping of Drosophila mutations using site-specific male recombination. Genetics *149*, 157–163.

Conlon, I., and Raff, M. (1999). Size control in animal development. Cell *96*, 235–244.

Creasy, C.L., and Chernoff, J. (1995). Cloning and characterization of a human protein kinase with homology to Ste20. J. Biol. Chem. *270*, 21695–21700.

Dan, I., Watanabe, N.M., and Kusumi, A. (2001). The Ste20 group kinases as regulators of MAP kinase cascades. Trends Cell Biol. *11*, 220–230.

Duman-Scheel, M., Weng, L., Xin, S., and Du, W. (2002). Hedgehog regulates cell growth and proliferation by inducing cyclin D and cyclin E. Nature *417*, 299–304.

Gao, X., and Pan, D. (2001). TSC1 and TSC2 tumor suppressors antagonize insulin signaling in cell growth. Genes Dev. *15*, 1383–1392.

Glantschnig, H., Rodan, G.A., and Reszka, A.A. (2002). Mapping of MST1 kinase sites of phosphorylation. Activation and autophosphorylation. J. Biol. Chem. *277*, 42987–42996.

Graves, J.D., Gotoh, Y., Draves, K.E., Ambrose, D., Han, D.K., Wright, M., Chernoff, J., Clark, E.A., and Krebs, E.G. (1998). Caspase-mediated activation and induction of apoptosis by the mammalian Ste20-like kinase Mst1. EMBO J. *17*, 2224–2234.

Green, D.R., and Evan, G.I. (2002). A matter of life and death. Cancer Cell *1*, 19–30.

Hanks, S.K., Quinn, A.M., and Hunter, T. (1988). The protein kinase family: conserved features and deduced phylogeny of the catalytic domains. Science *241*, 42–52.

Hay, B.A., Wassarman, D.A., and Rubin, G.M. (1995). Drosophila homologs of baculovirus inhibitor of apoptosis proteins function to block cell death. Cell *83*, 1253–1262.

Hisaoka, M., Tanaka, A., and Hashimoto, H. (2002). Molecular alterations of h-warts/LATS1 tumor suppressor in human soft tissue sarcoma. Lab. Invest. *82*, 1427–1435.

Johnston, L.A., and Gallant, P. (2002). Control of growth and organ size in Drosophila. Bioessays *24*, 54–64.

Justice, R.W., Zilian, O., Woods, D.F., Noll, M., and Bryant, P.J. (1995). The Drosophila tumor suppressor gene warts encodes a homolog of human myotonic dystrophy kinase and is required for the control of cell shape and proliferation. Genes Dev. *9*, 534–546.

Kango-Singh, M., Nolo, R., Tao, C., Verstreken, P., Hiesinger, P.R., Bellen, H.J., and Halder, G. (2002). Shar-pei mediates cell proliferation arrest during imaginal disc growth in Drosophila. Development *129*, 5719–5730.

Martin, S.J. (2002). Destabilizing influences in apoptosis: sowing the seeds of IAP destruction. Cell *109*, 793–796.

Neufeld, T.P., de la Cruz, A.F.A., Johnston, L.A., and Edgar, B.A. (1998). Coordination of growth and cell division in the *Drosophila* wing. Cell *93*, 1183–1193.

Newsome, T.P., Asling, B., and Dickson, B.J. (2000). Analysis of *Drosophila* photoreceptor axon guidance in eye-specific mosaics. Development *127*, 851–860.

Pan, D., and Rubin, G.M. (1997). Kuzbanian controls proteolytic processing of Notch and mediates lateral inhibition during *Drosophila* and vertebrate neurogenesis. Cell *90*, 271–280.

Richardson, H., O'Keefe, L.V., Marty, T., and Saint, R. (1995). Ectopic cyclin E expression induces premature entry into S phase and disrupts pattern formation in the Drosophila eye imaginal disc. Development *121*, 3371–3379.

Ryoo, H.D., Bergmann, A., Gonen, H., Ciechanover, A., and Steller, H. (2002). Regulation of Drosophila IAP1 degradation and apoptosis by reaper and ubcD1. Nat. Cell Biol. *4*, 432–438.

St John, M.A., Tao, W., Fei, X., Fukumoto, R., Carcangiu, M.L., Brownstein, D.G., Parlow, A.F., McGrath, J., and Xu, T. (1999). Mice deficient of Lats1 develop soft-tissue sarcomas, ovarian tumours and pituitary dysfunction. Nat. Genet. *21*, 182–186.

Stocker, H., and Hafen, E. (2000). Genetic control of cell size. Curr. Opin. Genet. Dev. *10*, 529–535.

Tapon, N., Harvey, K.F., Bell, D.W., Wahrer, D.C., Schiripo, T.A., Haber, D.A., and Hariharan, I.K. (2002). salvador promotes both cell cycle exit and apoptosis in *Drosophila* and is mutated in human cancer cell lines. Cell *110*, 467–478.

Taylor, L.K., Wang, H.C., and Erikson, R.L. (1996). Newly identified stress-responsive protein kinases, Krs-1 and Krs-2. Proc. Natl. Acad. Sci. USA *93*, 10099–10104.

Wolff, T., and Ready, D.F. (1993). Pattern formation in the Drosophila retina. In The Development of Drosophila melanogaster, M. Bate and A. Martinez Arias, eds. (Plainview, New York: Cold Spring Harbor Laboratory Press), pp. 1277–1325.

Xu, T., Wang, W., Zhang, S., Stewart, R.A., and Yu, W. (1995). Identifying tumor suppressors in genetic mosaics: the Drosophila lats gene encodes a putative protein kinase. Development *121*, 1053–1063.

Yoo, S.J., Huh, J.R., Muro, I., Yu, H., Wang, L., Wang, S.L., Feldman, R.M., Clem, R.J., Muller, H.A., and Hay, B.A. (2002). Hid, Rpr and Grim negatively regulate DIAP1 levels through distinct mechanisms. Nat. Cell Biol. *4*, 416–424.

Zallen, J.A., Peckol, E.L., Tobin, D.M., and Bargmann, C.I. (2000). Neuronal cell shape and neurite initiation are regulated by the Ndr kinase SAX-1, a member of the Orb6/COT-1/warts serine/threonine kinase family. Mol. Biol. Cell *11*, 3177–3190.

Note Added in Proof

In the accompanying paper, Harvey et al. present an independent characterization of the *hippo* gene. While our studies demonstrate that Hippo regulates DIAP1 at the transcriptional level, Harvey et al. present evidence suggesting that Hippo regulates DIAP1 through a posttranscriptional mechanism.